

Crust and upper mantle discontinuity structure beneath eastern North America

Aibing Li¹ and Karen M. Fischer

Department of Geological Sciences, Brown University, Providence, Rhode Island, USA

Suzan van der Lee²

Department of Terrestrial Magnetism, Carnegie Institution of Washington, Washington, D.C., USA

Michael E. Wyession

Department of Earth and Planetary Sciences, Washington University, St. Louis, Missouri, USA

Received 12 October 1999; revised 28 November 2000; accepted 20 August 2001; published 28 May 2002.

[1] Crust and mantle discontinuities across the eastern margin of the North American craton were imaged using *P* to *S* converted phase receiver functions recorded by the Missouri to Massachusetts Broadband Seismometer Experiment. Crustal structure constrained by modeling Moho conversions and reverberations shows a variation of Moho depth from a minimum of 30 km near the Atlantic coast to depths of 44–49 km beneath the western Appalachian Province and 38–45 km beneath the Proterozoic terranes in the west. The variation in crustal thickness is substantially greater than that required for local isostasy, unless lower crustal densities are $>3110 \text{ kg/m}^3$. In the upper mantle, *Ps* phases corresponding to a discontinuity at depths of 270–280 km were clearly observed beneath the eastern half of the array. Beneath the western third of the array, the receiver function stacks indicate more complex scattering, but weak *Ps* phases may be generated at depths of roughly 320 km. The transition between these two regions occurs across the eastern edge of the North American lithospheric keel imaged by tomography. The observed phases may be interpreted as conversions from the base of a low-velocity asthenosphere. *INDEX TERMS*: 7203 Seismology: Body wave propagation; 7205 Seismology: Continental crust (1242); 7218 Seismology: Lithosphere and upper mantle; 8120 Tectonophysics: Dynamics of lithosphere and mantle—general; *KEYWORDS*: Crustal structure, mantle discontinuity, eastern North America, receiver function

1. Introduction

[2] The goal of this paper is to image the Moho and upper mantle across the eastern edge of the North American craton using *Ps* conversions from seismograms recorded at the Missouri to Massachusetts Broadband Seismometer Experiment (MOMA) array. MOMA was a 1995–1996 Incorporated Research Institutions for Seismology Program for the Array Seismic Studies of the Continental Lithosphere (IRIS PASSCAL) deployment of 18 portable broadband seismometers between two permanent IRIS Global Seismic Network (GSN) stations at Cathedral Caves, Missouri (CCM), and Harvard, Massachusetts (HRV) [Fischer *et al.*, 1996] (Figure 1). Seismic tomography studies in North America [Grand, 1994; Grand *et al.*, 1997; van der Lee and Nolet, 1997] show that fast velocities extend to depths of more than 200 km beneath the western stations of the MOMA array, indicating a thick lithospheric “keel” (Figure 1). Beneath the easternmost stations in New England, the high-velocity lithosphere appears to be much thinner (100 km or less). The transition in lithospheric thickness correlates with the boundary between the Proterozoic cratonic crust in the west and the

Paleozoic Appalachian orogenic belt in the east. The last significant episodes of tectonic activity in this region are the Triassic and Jurassic rifting associated with the opening of the Atlantic Ocean [Klitgord *et al.*, 1989; Hatcher, 1989] and the magmatic activity associated with the Montereian hot spot at $\sim 120 \text{ Ma}$ [Sleep, 1990].

[3] This study focuses on constraining the crust and upper mantle discontinuities, whereas previous work with data from the MOMA array concentrated on discontinuities in the transition zone [Li *et al.*, 1998]. We model crustal structure across the MOMA array by matching observed and synthetic *P* to *S* conversions and reverberations from the Moho. Refraction studies have, in general, revealed a deeper Moho beneath the Appalachian Mountains [e.g., Braile, 1989; Braile *et al.*, 1989], and in the southern Appalachians the thickness of the crustal root appears to be greater than is required for local isostatic compensation of the heavily eroded topography [James *et al.*, 1968; McNutt, 1980]. Data from the MOMA array allow us to systematically investigate crustal thickness and isostasy in the northern Appalachians. The MOMA array also provides new constraints on Moho topography into the Proterozoic craton, a region where very few refraction studies exist. Also of particular interest are discontinuities at depths between 200 and 400 km, as they may reveal how lithospheric and asthenospheric structure varies across the edge of the keel. In addition, the phases from these depths are typically less contaminated by crustal reverberations than are earlier mantle arrivals. Discontinuities in this depth range have been observed in a number of continental regions [e.g., Revenaugh and Jordan, 1991; Revenaugh and Sipkin, 1994; Dueker and Sheehan, 1997; Yuan *et al.*

¹Now at Department of Geology and Geophysics, Woods Hole Oceanographic Institution, Woods Hole, Massachusetts, USA.

²Now at Institute of Geophysics, ETH Honggerberg (HPP), Zurich, Switzerland.

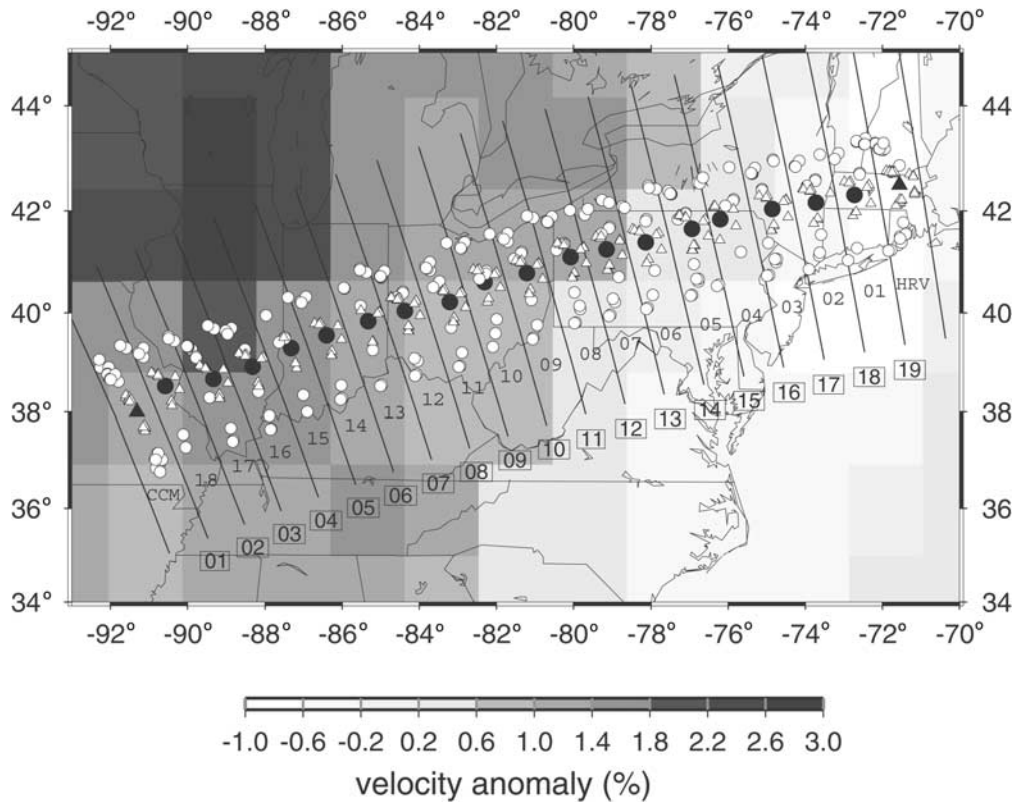


Figure 1. P to S conversion points at depths of 40 and 300 km along the MOMA array. The stations of the MOMA array (large solid circles) consisted of 18 broadband seismometers deployed from Missouri to Massachusetts between two permanent IRIS GSN stations CCM and HRV (large solid triangles). P_s conversion points are plotted as small open triangles and circles for conversion depths of 40 and 300 km, respectively. Station names are shown in each bin where the corresponding station is located. Only the number for each MOMA station is plotted. The full name of a MOMA station is “MM” followed by the number. Bin numbers with rectangular frames are given at the southern end of each bin. The shaded background is the S wave velocity anomaly at the depth of 175–250 km from seismic tomography by *Grand et al.* [1997]. The eastern margin of the continental keel is marked by the west to east decrease in velocity anomaly and is well sampled by P to S conversions.

al., 1997; *Bostock*, 1997; *Owens et al.*, 2000; *Sheehan et al.*, 2000]. Here we explore their existence beneath eastern North America.

2. The Transition Zone Beneath the MOMA Array

[4] Previous work on transition zone discontinuities using data from the MOMA array provides context for the crust and mid-upper mantle discontinuity images in this study. *Li et al.* [1998] found that the 410-km discontinuity (hereinafter referred to as the 410) is relatively flat to both the north and south of the array and that the transition zone thickness is nearly uniform to the north, where the P_s conversion points extend the farthest into the mantle below the fast velocity keel. Considering the effects of temperature alone, this minimal topography on the 410, combined with estimates of uncertainties in discontinuity depth, indicates that thermal variations of more than 100°C–150°C do not impinge on the 410. The depth of the 410 is increased by higher olivine Mg content [*Bina and Wood*, 1987; *Katsura and Ito*, 1989; *Akaogi et al.*, 1989], and if the keel, which is thought to have a higher Mg number than the surrounding mantle, reaches the phase transition, this effect could mask an additional thermal variation of at most 65°C, assuming an average Mg number of 92.3 for the North American keel [*Schmidberger and Francis*, 1999] and an

“oceanic” Mg number of 90.8 [*Boyd*, 1989]. However, tomographic images [*van der Lee and Nolet*, 1997] suggest that the keel does not extend to depths of more than 250–300 km beneath the MOMA array. Therefore cold mantle downwelling related to the keel is largely confined in the upper mantle, at least at this point in time. Whereas *Li et al.* [1998] determined that the 660-km discontinuity (hereinafter referred to as the 660) is relatively flat to the north of the MOMA stations, a roughly 20 km depression of the 660 occurs to the south of the western stations. This depression is correlated with a localized fast velocity anomaly at depths of 525–800 km [*Grand et al.*, 1997], which broadens into the fast slab-like anomaly interpreted as the subducted Farallon plate [*Grand*, 1994; *Grand et al.*, 1997] at greater depths. The 660 depression may therefore reflect locally cold temperatures within the Farallon plate.

3. Data and Method

3.1. Receiver Functions

[5] The data used in this study are P_s conversions recorded by the MOMA stations from events that occurred between February 1995 and March 1996 with magnitudes larger than 5.8 and distances from 40° to 90°. For the two permanent IRIS GSN stations, HRV and CCM, we analyzed events that occurred over 5 years from 1991 to 1995. Most MOMA

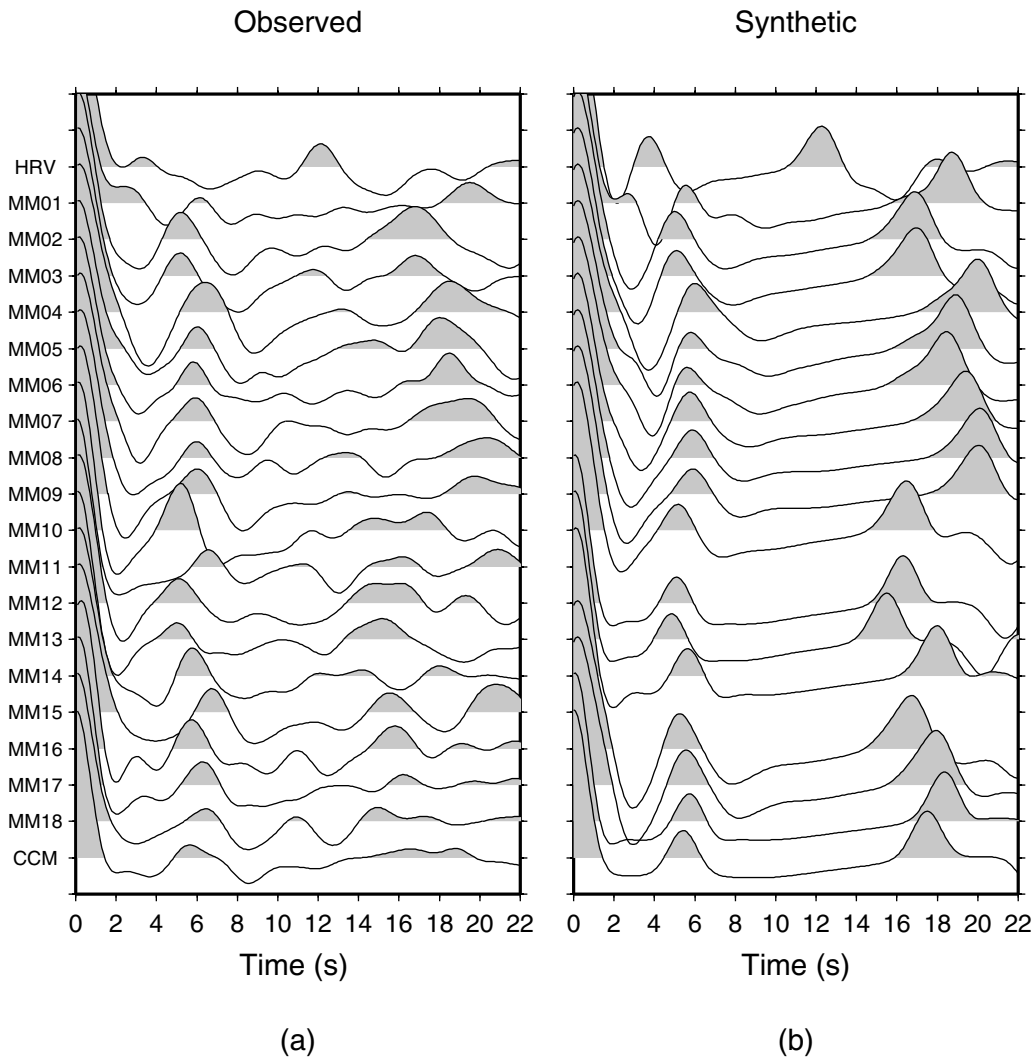


Figure 2. Observed and synthetic receiver functions including Moho conversions and reverberations. (a) Stacked crustal receiver functions for all stations along the MOMA array. P_{ms} phases (positive polarity) arrive at roughly 5 s, and the differences in their timing indicate a variation in crustal structure beneath the array. (b) Best fitting synthetic receiver functions for each station obtained with models containing sedimentary layers and one crustal basement layer. Synthetics for MM11 and MM15 are not shown; see text for discussion. Receiver function stacks are filtered with a 0.05 to 1 Hz band pass.

stations recorded good waveforms from 8 to 16 sources except MM15, for which only 4 useful events exist. The distribution of back azimuths is dominated by two groups, 150° – 180° (southeast Pacific and South American events) and 320° – 340° (north and northwest Pacific events). A small number of useful events lie at back azimuths of 40° – 60° for each station. This distribution is shown in Figure 1 by the locations of P to S conversion points. Three-component seismograms for each event were windowed at ~ 10 s before and 120 s after the P arrival and filtered with frequency bands from 0.03 to 1 Hz and from 0.05 to 1 Hz. To obtain receiver functions, we deconvolved the vertical component seismogram from the radial component [Langston, 1979; Owens and Crosson, 1988; Ammon, 1991]. The deconvolution was multiplied by the transform of a Gaussian, whose width is controlled by a parameter, to limit the final frequency band [Langston, 1979]. We set a value of 1 for the controlling parameter of the Gaussian to exclude high-frequency signals. The deconvolution suppresses waveform variations from the earthquake source and

nondiscontinuity path effects and enhances the amplitude of P to S conversions and reverberations generated beneath the station.

3.2. P to S Conversion Point Binning

[6] P to S conversions and reverberations from the Moho are typically visible on individual receiver functions because of the large contrast in velocity between the crust and mantle, whereas conversions from mantle discontinuities are harder to observe. To increase the P_s signal-to-noise ratio and to extract information about both crust and mantle discontinuities, we stacked individual receiver functions as a function of P to S conversion point locations after corrections for phase move out in the AK135 radial velocity model [Kennett *et al.*, 1995]. Mantle phases were also corrected for velocity heterogeneity in the crust and mantle. Figure 1 shows the distribution of P to S conversion points at depths of 40 and 300 km calculated by ray tracing through the AK135 velocity model. The conversion points from deeper discontinuities sample larger areas in which conversion points may correspond to different stations.

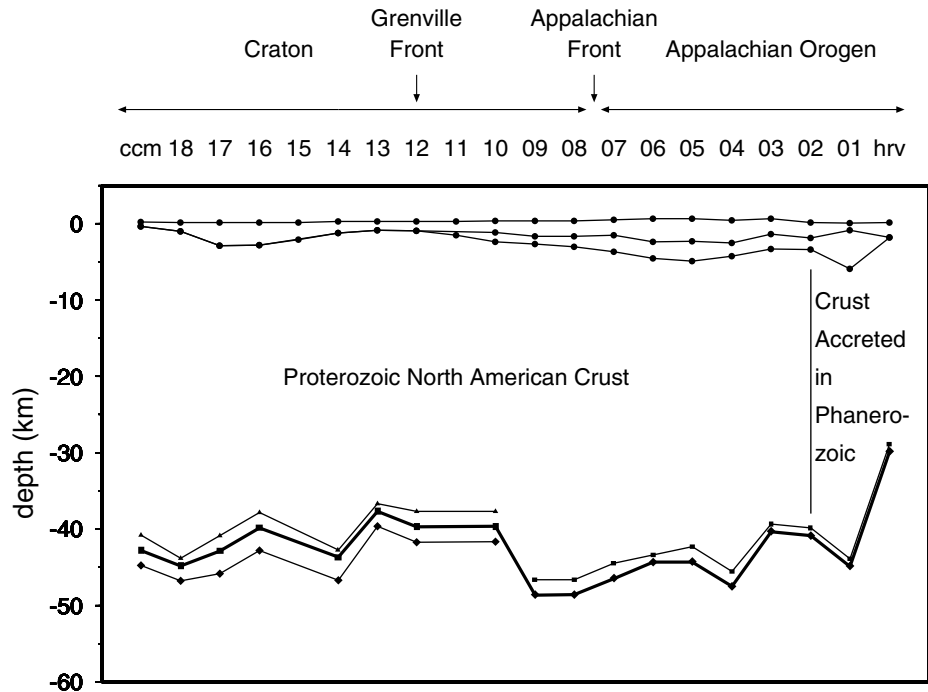


Figure 3. Station elevations (solid circles), thickness of sedimentary layers (solid circles), and Moho topography beneath the MOMA array. The total thicknesses of the sedimentary rocks are from published maps [Flawn *et al.*, 1967; Shumaker and Wilson, 1996; Hinze, 1996]; their relative thicknesses and total crustal thickness were determined by modeling P_{ms} phases and Moho reverberations beneath each station. Three crustal basement velocity combinations were used for the western stations, and two were used for the eastern stations. Triangles indicate a V_p equal to 6.6 km/s and a V_p/V_s ratio of 1.84, squares indicate a V_p equal to 6.6 km/s and a V_p/V_s ratio of 1.8, and diamonds indicate a V_p equal to 6.5 km/s and a V_p/V_s ratio of 1.73. The heavy line indicates the models that provide the best fit to regional groupings of stations.

Therefore, to extract lateral variations in mantle discontinuity structure, we stacked receiver functions whose conversion points on a given conversion surface fall into the same geographic bin, the common midpoint stack technique applied to P_s conversions from broadband arrays by Dueker and Sheehan [1997, 1998]. In this study, we divided the MOMA array into 19 bins of equal width with each bin overlapping its neighbors by 50%. One disadvantage of this approach is the assumption that conversions are generated at planar discontinuities. If significant scattering from discontinuity topography or other two- and three-dimensional structure exists, it may create bias in apparent discontinuity amplitudes and timing and perhaps result in spurious phases. In some cases, such artifacts may be avoided by using migration methods that account for three-dimensional scattering [Shearer *et al.*, 1999; Sheehan *et al.*, 2000]. However, given that the MOMA array was roughly linear and had a station spacing of ~ 90 km, the advantages of true migration over the simpler stacking method used here are unclear. In any case, we treat as significant only those stacked P_s phases whose move out is consistent with conversions from a planar surface and which are fairly continuous across several neighboring bins.

4. Crustal Structure Beneath the MOMA Array

4.1. Observations

[7] P to S conversions at the Moho show strong amplitudes due to the Moho's large velocity contrast and are clearly visible even on individual receiver functions. Assuming a conversion depth of 40 km, Moho conversion points for events recorded at one station sample a relatively small area around the station (Figure 1). In

order to obtain information about average crustal structure, we stacked radial receiver functions together by station. Figure 2a shows the crustal receiver function stacks over a time window at 0–22 s for all stations of the array. The phases at 0 s with large amplitudes are direct P wave arrivals. Certain P phases manifest apparent offsets from zero time due to the effects of thick sedimentary layers. Such lags are observed at MM06 to MM08 and MM15 to MM17 that are located in the Appalachian basin and Illinois basin, respectively. For most stations, P_{ms} phases arrive at roughly 5 s and the Moho reverberations $PpPs$ range from 15 to 20 s. P_{ms} phases and Moho reverberations are similar for certain groups of adjacent stations, for instance, MM02–MM03, MM04–MM09, MM12–MM13, and MM15–CCM, but clear differences exist across the array. The receiver function at HRV displays a significantly earlier P_{ms} phase and Moho reverberation than those at other stations, suggesting a much shallower Moho. The phases at roughly 7 s on the stacks for MM11 and MM15 seem too late for Moho conversions, and they may include interference between P_{ms} and reverberations from discontinuities in the shallow crust. The Moho reverberations at MM11 and MM15, which would be less affected by shallow discontinuities than the P_{ms} phases, are similar to reverberations at adjacent stations.

4.2. Modeling Moho Conversion and Reverberation Phases

[8] To obtain the crustal velocity structure beneath each station, we forward modeled P_{ms} and Moho reverberations using synthetic receiver functions. Simple one-dimensional velocity models were constructed including one or two layers of sedimentary rocks and one crustal basement layer. The total sedimentary rock thickness beneath each station was obtained from published maps [Flawn *et*

al., 1967; Shumaker and Wilson, 1996; Hinze, 1996] and varied from 0.6 to 6.0 km (Figure 3). P wave velocity was assumed to be 4.5 km/s in the top sedimentary rock layer and 5.3 km/s in the bottom layer. These velocities are based on the range of P wave velocities in consolidated sediments (4.0–5.3 km/s) quoted by Mooney *et al.* [1998] and are broadly consistent with values from individual profiles summarized by Braile *et al.* [1989]. A V_p/V_s ratio of 1.73 was assumed in the sedimentary layers, and their relative thicknesses were determined by matching the shapes of observed P and P_{ms} phases. Ranges of plausible values for V_p and V_p/V_s in the crustal basement layers were determined from extensive compilations of individual refraction profiles [Hutchinson *et al.*, 1983; Braile, 1989; Braile *et al.*, 1989; Mooney and Braile, 1989; Musacchio *et al.*, 1997]. The refraction data indicate that V_p and V_p/V_s values are on average higher in the Proterozoic crust of the Grenville Province and the Central Plains than in Appalachian crust. However, because only very limited segments of the crust beneath the MOMA array are directly sampled by refraction profiles and because individual refraction profiles manifest considerable variation even within given tectonic terranes, we did not assume different crustal velocities for different segments of the array. Rather, we modeled all observed crustal receiver functions with three V_p and V_p/V_s combinations in the crustal basement layer: $V_p = 6.5$ km/s and $V_p/V_s = 1.73$, $V_p = 6.6$ km/s and $V_p/V_s = 1.80$, and $V_p = 6.6$ km/s and $V_p/V_s = 1.84$.

[9] For each station and for each basement, V_p , and V_p/V_s combination, the relative thickness of the two sedimentary layers, and the total crustal thickness were systematically varied until the synthetic receiver functions best matched the shapes and timing of P , P_{ms} , and the first Moho reverberation. The best fitting depths to these crustal interfaces are shown in Figure 3. In general, the basement V_p of 6.5 km/s and V_p/V_s ratio of 1.73 provided a much better fit to the receiver functions from the eastern half of the array (HRV to MM09), while a V_p of 6.6 km/s and a V_p/V_s ratio of 1.80 more closely matched the western stations (MM10 to CCM). Basement layer thickness is most sensitive to basement V_p/V_s values, and the range of Moho depths obtained with the different V_p/V_s values is a good representation of the uncertainty in Moho depth at a given station. Because a V_p of 6.6 km/s and a V_p/V_s ratio of 1.84 did not yield acceptable fits to the HRV–MM09 receiver functions, crustal thicknesses for these basement velocities are shown only for MM10–CCM. Synthetic receiver functions from the velocity models with best fitting regional V_p and V_p/V_s values are displayed in Figure 2b. At most stations, the arrivals of the synthetic P_{ms} phases and the Moho reverberations match the timing of the observed phases (Figure 2a) well, although in a few isolated cases, another V_p/V_s value would provide a better fit (for instance a V_p/V_s of 1.80 at MM04). For two stations, MM11 and MM15, none of the basement velocity combinations provided a good fit to both the P_{ms} phase and the Moho reverberation, although models with the highest V_p/V_s ratio (1.84) came the closest. The Moho reverberations at these two stations arrive at times comparable to adjacent stations, while the apparent P_{ms} phases are significantly delayed, which may indicate complex velocity structures in the shallow crust. We therefore did not rely on independent synthetic receiver functions for these two stations and instead used the MM12 crustal model for MM11 and the MM16 crustal model for MM15, when calculating move out corrections for deeper discontinuities. Although the amplitude of the synthetic P_s phases provides a reasonable fit to the observations, the synthetic reverberation amplitudes are, in general, too large. However, this is a common outcome of modeling observed receiver functions with planar models, which simplify real crustal structure, as reverberation amplitudes are particularly sensitive to deviations from planar structure.

[10] We summarize possible crustal models in Figure 3. For the best fitting regional basement velocities the thickness of crust has an average value of 43.0 ± 4.5 km and varies from 30 km near

the Atlantic margin (HRV) to a maximum of 49 km near the boundary between the Appalachian and Grenville Provinces (MM08 and MM09). The crust beneath MM04–MM09 has an average thickness of 47.2 ± 1.8 km and is substantially thicker than the crust beneath MM10–CCM (average thickness of 41.6 ± 2.4 km) or beneath MM03–HRV (average thickness of 39.2 ± 6.4 km). The observed timing of the P_{ms} phases and Moho reverberations clearly differentiates these groups of stations, particularly the variation in crustal thickness between MM04–MM09 and MM10–CCM.

4.3. Crustal Structure, Orogeny, and Isostasy

[11] Numerous refraction surveys have documented similar crustal thickening from 30–35 km near the Atlantic Coast to >40 km in the continental interior [Costain *et al.*, 1989; Mooney and Braile, 1989; Braile, 1989; Braile *et al.*, 1989]. However, while the crustal thickness variations obtained in this study loosely agree with a number of interpolations of refraction data [Braile, 1989; Braile *et al.*, 1989], other studies show monotonic thickening of the crust from east to west beneath the MOMA array [Mooney and Braile, 1989; Mooney *et al.*, 1998]. The observation that the thickest crust lies beneath MM04–MM09 is broadly consistent with a number of more localized studies. Hawman and Phinney [1992] found Moho depths of 47–52 km beneath eastern Pennsylvania, whereas beneath station CCM, Langston [1994] determined a crustal thickness of 40 km. In the interpretations of Hutchinson *et al.* [1983] and Costain *et al.* [1989] the crust beneath the Appalachian highlands is thicker than beneath the Grenville Province.

[12] Crustal thickness variations correlate only loosely with different tectonic provinces. Crustal thickness in the western or external portion of the Appalachian Province (MM03–MM07) is on average greater than in the Grenville and central U.S. Proterozoic Provinces (MM08–MM11 and MM12–CCM, respectively). Western Appalachian crust is also on average thicker than the crust of the eastern portion or internal Appalachians spanned by MM02–HRV, much of which was rifted during the Triassic and Jurassic opening of the Atlantic. However, the rapid thinning of the crust between MM09 and MM10 actually occurs ~ 200 km to the west of the Appalachian Front as mapped by Hoffman [1989] and even farther west of the surficial limit of substantial Appalachian deformation given in other tectonic studies [Rast, 1989; Rankin, 1994]. If the deeper Moho beneath the western Appalachians is related to Appalachian orogenesis (i.e., thickening of the Grenville basement, which lies beneath the sedimentary cover rocks of the external Appalachians), then the constraints on Moho depth obtained in this study suggest that at depth, this deformation extends west of the surface extent of the Appalachian cover rocks. Such an interpretation would contradict geological models which indicate only shallow crustal deformation associated with the Appalachian orogeny in this region. Alternatively, some components of the observed Moho topography may predate the Appalachian orogeny. For instance, the rapid decrease in crustal thickness between MM09 and MM10 roughly correlates with an apparent change in the dip of upper crustal and midcrustal reflectors (east dipping reflectors to the west and west dipping reflectors to the east) [Pratt *et al.*, 1989] and with the Akron magnetic boundary [Rankin *et al.*, 1993]. These coinciding features may represent a Proterozoic age suture in the Grenville basement [Rankin *et al.*, 1993]. It is unclear whether the Moho topography observed today across the potential suture predated or developed during the Appalachian orogeny. In either case, the suture may have acted as a zone of weakness, allowing crustal thickening associated with the Appalachians to penetrate farther to the west. Another interpretation is that the Moho topography, and possibly the reflectors and magnetic boundary, are associated with the epeirogenic deformation that formed the Cincinnati Arch [cf. Marshak and van der Pluijm, 1997].

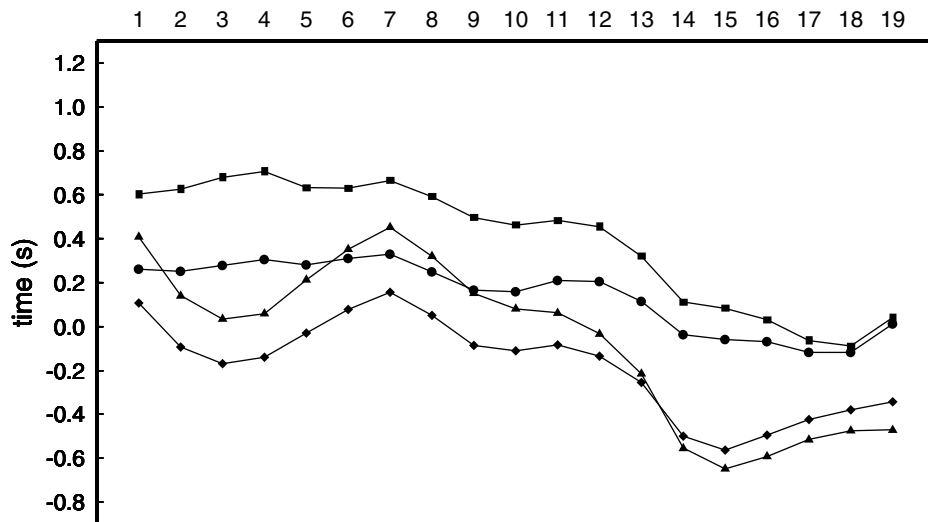


Figure 4. Average timing corrections for lateral heterogeneity in the crust and mantle for conversions at the depth of 300 km across the MOMA array. The squares and the circles are for the model by *Grand et al.* [1997] with $\delta[\ln(V_s)]/\delta[\ln(V_p)]$ values of 2.5 and 1.0, respectively. The triangles and diamonds are for the NA95 model of *van der Lee and Nolet* [1997] with $\delta[\ln(V_s)]/\delta[\ln(V_p)]$ values of 2.5 and 1.0, respectively.

[13] Local isostatic compensation of surface topography by a uniform density crust would predict Moho depths that are anticorrelated with surface topography. Such a relationship is not observed on a station-by-station basis across this region, but at scales of a few hundred kilometers, surface topography and crustal thickness are roughly anticorrelated. For example, the average elevation of MM04–MM09, the region with the thickest crust, is 0.26 km greater than that of MM10–CCM and 0.24 km greater than that of MM03–HRV. However, crustal thickness variations are larger than required to locally compensate the subdued surface topography with a uniform density crust, unless the density contrast between the crust and mantle is small. Crustal thickness beneath MM04–MM09 is 5.6 km thicker than that beneath MM10–CCM, assuming the best fitting regional values of crustal basement velocities (heavier line in Figure 3), and 3.7 km thicker if a V_p of 6.6 km/s and a V_p/V_s ratio of 1.80 are assumed at all stations. These values imply that the density contrast between the mantle and the thickened crust is no more than 120–190 kg/m³, assuming local isostasy and a surface topography density of 2670 kg/m³. Given a mantle density of 3300 kg/m³, this crustal buoyancy indicates a crustal density in excess of 3110 kg/m³. If smaller crustal densities are assumed, the observed crustal thickness would such “overcompensate” the topography, a scenario that has been suggested for the southern Appalachians [*James et al.*, 1968; *McNutt*, 1980]. In contrast, studies in the southern Rockies [*Sheehan et al.*, 1995] and the Sierra Nevada [*Keller et al.*, 1998] have found that crustal thickness variations are too small to isostatically balance the topography of these mountains, and they conclude that low-density mantle must provide some support.

[14] Could lateral gradients of density in the crust and/or mantle beneath the MOMA array make a significant contribution toward local isostasy? It is possible that the crust beneath MM04–MM09 is denser than that beneath MM02–HRV, since the surface expression of the suture between the Grenville and the Appalachian Provinces lies near MM02, and Grenville basement appears to have a higher density [*Musacchio et al.*, 1997]. It is less likely that the average crustal density is higher beneath MM04–MM09 than beneath MM10–CCM, since the MM10–CCM receiver function stacks are typically better modeled by higher V_p/V_s ratios. For upper mantle density gradients to

counterbalance isostatic support from the crust and allow smaller crustal densities, lower-density buoyant mantle material would be required beneath MM10–CCM. If the velocity contrast between thick lithospheric keel and eastern mantle [cf. *Grand*, 1994; *Grand et al.*, 1997; *van der Lee and Nolet*, 1997] were scaled to temperature, resulting density anomalies would detract from isostatic balance. Chemical depletion may contribute to keel buoyancy [*Jordan*, 1978, 1988], but the net effect of thermal and chemical keel anomalies would need to be positively buoyant to offset the relatively thick crust beneath the modestly elevated topography outside of the keel.

[15] Although modeling of gravity data is inherently nonunique, it does provide a means of testing specific density models. Assuming that support of the topography is largely crustal and that large lateral variations in density do not occur, observed crustal thicknesses predict a decrease in Bouguer gravity anomaly of –40 mGal or more beneath MM04–MM09 unless crustal densities on the order of 3000 kg/m³ or more are assumed within the thickened crustal root. Observed Bouguer gravity anomalies [*Hittelman et al.*, 1990] in the vicinity of the MOMA array do not manifest such negative values beneath MM04–MM09 and are more consistent with crustal density values of roughly 3100 kg/m³ as well as local isostatic compensation.

5. Mantle Discontinuities

5.1. Corrections for Lateral Heterogeneity

[16] As shown in section 4, large variations in crustal structure exist across the MOMA array, and strong lateral velocity gradients have been imaged with seismic tomography [cf. *Grand*, 1994, *Grand et al.*, 1997; *van der Lee and Nolet*, 1997]. It was therefore imperative to account for the effects of lateral heterogeneity in the crust and upper mantle on the travel times of P and P_s phases when the receiver functions were stacked to image mantle discontinuities.

[17] Corrections for lateral heterogeneity were based on the three-dimensional S wave velocity model of *Grand et al.* [1997] (hereinafter referred to as the Grand model), modified to include the best fitting crustal structure beneath the station (described in section 4). P wave model velocities were obtained by scaling each S wave model with V_p/V_s ratios from the AK135 model and

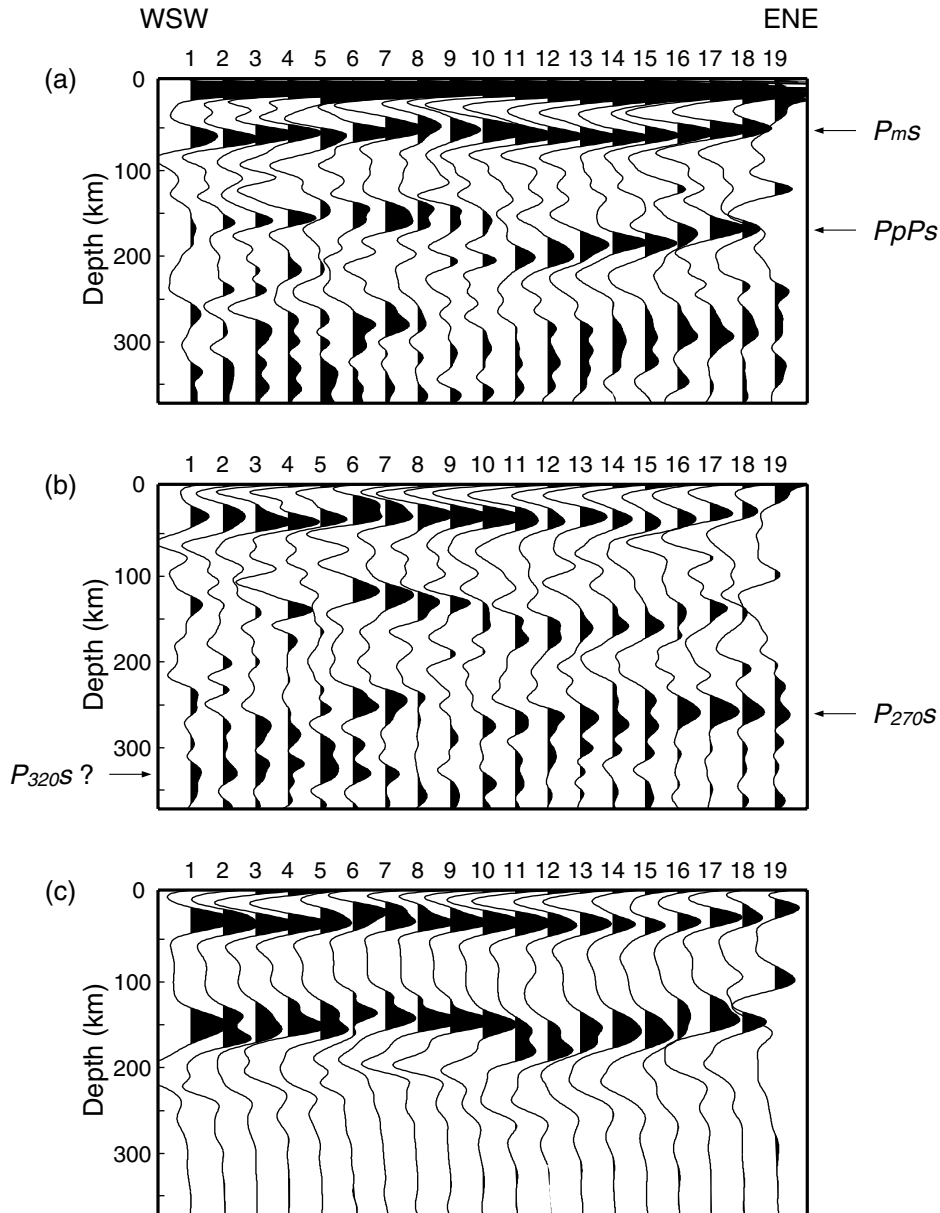


Figure 5. (a) Stacks of receiver functions with corrections for the move out of $PpPs$ Moho reverberations assuming a Moho depth of 40 km. Although the data are stacked at a reverberation move out, time is converted to conversion depth to be consistent with Figures 5b and 5c. (b) Stacks of receiver functions with a move out correction for conversions at 300 km depth calculated from the AK135 velocity model. Corrections for lateral heterogeneity in the mantle and crust were obtained from the Grand model assuming a $\delta[\ln(V_s)]/\delta[\ln(V_p)]$ value of 1.0, and the crustal model that best fits crustal conversions recorded at the given station. (c) Stacks of synthetic receiver functions calculated from models with the best fitting crustal structure and a half-space. Note that there is no positive polarity phase at depth 270–320 km on synthetic stacks, indicating the phases in Figure 5b are P to S conversions from discontinuities in the upper mantle. All receiver function stacks are filtered with a 0.03 to 1 Hz band pass.

$\delta[\ln(V_s)]/\delta[\ln(V_p)]$ ratios of 1.0. A $\delta[\ln(V_s)]/\delta[\ln(V_p)]$ value of ~ 1.0 is suggested by comparison of recent high-resolution tomographic inversions for global P wave and S wave velocities [Grand et al., 1997; Van der Hilst et al., 1997] and corresponds to experimental measurements of thermally induced velocity variations in mantle minerals [Isaak, 1992]. To estimate errors on the depths of mid-upper mantle discontinuities from our chosen model, we also computed corrections for lateral heterogeneity from model NA95, a S wave velocity model for North America obtained by van der Lee and Nolet [1997] from Rayleigh wave data. In addition to a

$\delta[\ln(V_s)]/\delta[\ln(V_p)]$ value of 1, a value of 2.5 was tested as a high-end estimate of thermally induced velocity variations [Agnon and Bukowski, 1990]. The Ps - P time corrections at conversion depth of 300 km for the four versions of mantle heterogeneity are shown in Figure 4. Although the absolute values of the corrections change, the patterns are similar for different mantle models. The corrections become larger and more positive from east to west across the array, reflecting the thicker and faster keel beneath the western stations. This trend shifts apparent discontinuity depths down by as much as 8 km. Considering the effects from different models, errors on the

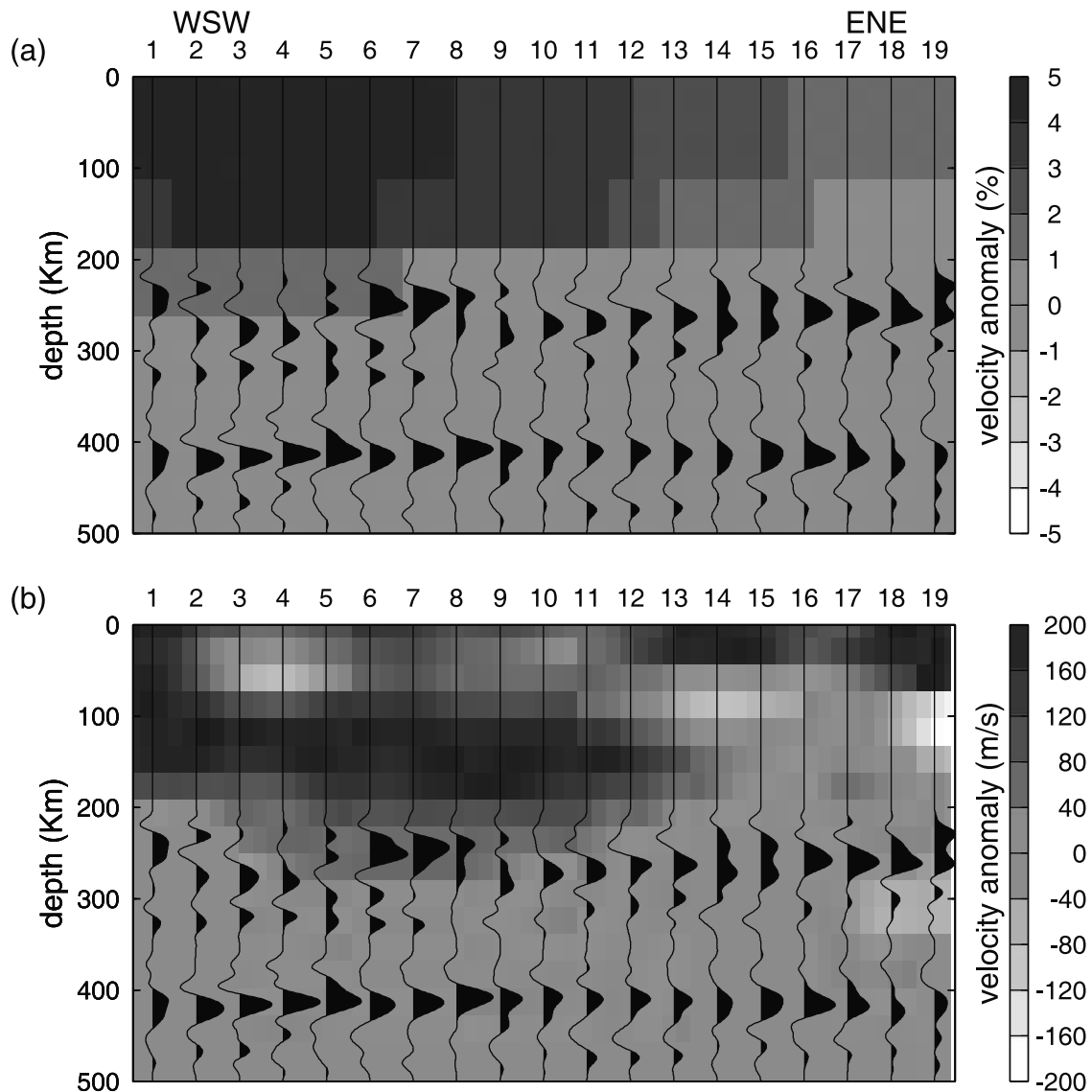


Figure 6. Receiver functions including conversion depths at 300 and 410 km on a background of velocity anomaly from (a) the Grand model and (b) the NA98 model. Data in the 200–350 km depth range are stacked with move out corrections for conversions at 300 km, and data in the 350–500 km depth range are stacked with move out corrections for conversions at 410 km. Earlier arriving phases are not shown. The keel is imaged by a broad lateral gradient in the Grand model, while it is a sharper feature in the NA98 model. The keel is confined above 300 km in both models, which is consistent with the relatively flat discontinuity at 410 km. Receiver function stacks are filtered with a 0.05–1 Hz band pass. See color version of this figure at back of this issue.

apparent discontinuity depths obtained from the Grand model with a $\delta[\ln(V_s)]/\delta[\ln(V_p)]$ of 1.0 are roughly ± 4 km. Variations in crustal V_p/V_s of the magnitude shown in Figure 3 would introduce another ± 2 km of uncertainty in the discontinuity depth estimates.

5.2. Observed Upper Mantle Phases

[18] On stacked receiver functions across the MOMA array we observed relatively strong positive polarity phases at 26–33 s. We applied a series of tests to the data to determine whether these phases are P to S conversions from upper mantle discontinuities at depths of 270–320 km or multiple reverberations from the base of sedimentary layer and the Moho. We stacked the receiver functions with the move out of the $PpPs$ Moho reverberation (Figure 5a) and with the move out for P to S conversions from 300 km depth (Figure 5b).

These stacks were corrected for the Grand mantle velocity model, assuming the best fitting crustal structures described in the previous section, and a $\delta[\ln(V_s)]/\delta[\ln(V_p)]$ ratio of 1.0.

[19] As expected, the amplitude of $PpPs$ is enhanced when it is stacked at its correct move out (Figure 5a) and diminished when it is stacked at the P_{300s} move out, which has a slope of opposite sign (Figure 5b). In contrast, the energy arriving after $PpPs$ stacks more coherently at the P_{300s} move out, indicating that a substantial component of this signal originates at a mid-upper mantle discontinuity. We also tried stacking the data using the move outs of a number of other crustal reverberations, and these stacks looked nearly identical to Figure 5a. The $PpPs$ phase does not disappear in Figure 5b because the range of distances and ray parameters represented in the data is fairly limited. This argument also explains why conversions from depths of roughly 300 km still

appear prominently, albeit with smaller amplitudes and less coherence, in Figure 5a.

[20] To further test whether the later phases are really P to S conversions, and not sidelobes of $PpPs$ or another crustal phase, we calculated synthetic seismograms for models with our best fitting crustal structure over a mantle half-space and processed them in exactly the same way as we processed the data. Figure 5c shows the synthetic receiver functions stacked at the P_{300S} move out. No positive polarity phase appears in the 270–320 km depth range. Comparing the three diagrams in Figure 5, we conclude that it is reasonable to interpret the positive polarity phases at depths of 270–320 km as P to S conversions.

[21] A band-pass filter of 0.03–1 Hz was applied to the data and synthetics in Figure 5. The 270–320 km phases are actually clearer beneath the eastern stations with a band-pass filter from 0.05 to 1 Hz (Figure 6) because some records have noise with strong amplitude at 20–30 s. In the comparisons of Figure 5 we adopted a somewhat wider band pass to minimize the potential for sidelobe artifacts. Beneath the westernmost stations, the 0.05–1 Hz filter reduces the amplitude of the deepest apparent phase at \sim 320 km. We also stacked the receiver functions using move outs for conversion depths of 250, 300, and 350 km. These experiments yielded similar waveform shapes, while the depths implied by the timing of the phases shifted by less than \pm 5 km relative to Figure 5b.

[22] The apparent discontinuity structure (Figures 5b and 6) shows a striking east to west variation. Beneath the eastern stations (bins 16–19), a strong positive polarity phase occurs at depths of roughly 270 km. The phase is continuous but relatively weaker beneath bins 9–15 and deepens toward the west to \sim 280 km beneath bin 10. More complex scattering occurs beneath the western third of the array (bins 1–7). A weak phase appears at depths of roughly 320 km, but its amplitude is frequency-dependent, and we judge it to be less robust than the 270–280 km phase observed in the east. The energy arriving in the 200–300 km window in bins 1–7 exhibits neither the move out nor the continuity between bins expected from conversions at a quasi-planar discontinuity. This is particularly true of the strong positive phases at \sim 250 km in bins 6 and 7 which originate from a very limited range of back azimuths and distances. The transition between bins 1–7 and bins 9–19 is associated with the eastern edge of the craton, and the variation in scattering likely reflects differences between the Proterozoic lithosphere in the west and the Phanerozoic lithosphere in the east.

5.3. Possible Sources for the Upper Mantle Discontinuities

[23] Upper mantle discontinuities have been investigated for decades. A 220-km discontinuity in the upper mantle was first suggested by Lehmann [1961] and later incorporated by Dziewon-ski and Anderson [1981] into the preliminary reference Earth model (PREM). However, debate still exists as to whether the Lehman (L) feature is a global discontinuity. For instance, Shearer [1991] found no evidence for an L discontinuity in global stacks of long-period waveform data. Evidence is accruing that a variety of upper mantle discontinuities are observed in the 200–350 km depth range on a regional basis, including analyses of Ps conversions from the Snake River Plain, Tibet, the Canadian Shield, Tanzania, and Iceland [Dueker and Sheehan, 1997; Yuan et al., 1997; Bostock, 1997; Owens et al., 2000; Shen et al., 1998; Sheehan et al., 2000]. Using ScS reverberations, Revenaugh and Jordan [1991] observed a number of upper mantle discontinuities, one of which is reminiscent of our observations in that it ranges in depth from 210 km beneath the Phanerozoic orogenic zones of Australia to more than 300 km in the stable continental interior. Revenaugh and Sipkin [1994] observed a similar discontinuity deepening from 250 km beneath the NW Fold Belt of China to 300 km beneath the Tibetan Plateau. This phase has been attributed to a transition from a mechanically strong, anisotropic layer to a weaker and isotropic layer, both of which are contained in a coherent

continental “tectosphere” [Revenaugh and Jordan, 1991; Revenaugh and Sipkin, 1994; Gaherty and Jordan, 1995; Gaherty et al., 1999]. Other studies have suggested that certain mid-upper mantle discontinuities represent the base of a low-velocity zone (LVZ) [Lehmann, 1961; Anderson, 1979; Leven et al., 1981; Hales, 1991; Sheehan et al., 2000].

[24] The viability of these different models for the phases imaged beneath the MOMA array may be partially assessed by a comparison of the observed conversions with three-dimensional (3-D) tomographic models. Figure 6 shows the phases stacked for an assumed conversion depth at 300 km on the color background of the shear velocity anomalies from the Grand model and the NA98 model. NA98 was obtained by application of the partitioned waveform inversion method to the waveform data set employed by van der Lee and Nolet [1997] enhanced with waveforms recorded by the MOMA array. In particular, the S and surface wave trains of the vertical component data from the 14 April 1995 magnitude 5.7 event in Texas and of the transverse component data from the 28 August, 1995 magnitude 6.9 event in the Gulf of California were fitted and included in the waveform inversion for NA98. These events are located near the great circle through the MOMA array and thus provide optimal constraints on the variation in upper mantle structure along the MOMA array (Figure 6b). These MOMA waveform data confirm the features of model NA95 along the MOMA great circle in an overall sense but with enhanced resolution, in particular in the 200–300 km depth range. The strength and overall pattern of heterogeneity are very similar in NA98 and NA95. In the Grand model (Figure 6a) the eastern edge of the cold and presumably fast North America keel appears as a broad and smooth west to east decrease in velocity, whereas the edge of the keel is a sharper and more complex gradient in NA98 (Figure 6b). Phases stacked assuming a conversion depth at 410 km are also shown in Figure 6 and reveal little topography on this discontinuity [Li et al., 1998]. As discussed in section 5.2, the 270–280 km phases in bins 9–19 are robust features of the receiver function stacks. The 320-km phases in bins 1–7 are somewhat more ephemeral but may represent a single discontinuity. In any case, the scattering beneath the western stations is more complex. The clear variation in the character of the 270–320 km scattering (bins 9–19 versus bins 1–7) roughly correlates with the eastern edge of the thick subcratonic lithosphere.

[25] In both tomography models, anomalously fast velocities, representative of the keel, are concentrated at depths of $<$ 250 km beneath the western stations and at depths of $<$ 100 km beneath the eastern stations. Thus a sublithospheric discontinuity is clearly required to explain the 270–280 km phase in the east. Some of the scattering beneath the western stations may occur in the lithosphere, but if the 320-km phase is real, it is likely of sublithospheric origin. A plausible explanation for the 270–280 km phase in the east is that it is a conversion from the base of an asthenospheric LVZ. Is it possible that this type of LVZ extends beneath western stations within the North American craton where the lithosphere is up to 250 km thick? The absolute velocities for the Grand model, in fact, reveal a LVZ at depths of \sim 200 to \sim 300 km across the array, although this LVZ is a feature of the one-dimension starting model. Absolute velocities in NA98 contain gentler gradients in the 250–300 km depth range but are not inconsistent with a deep asthenospheric LVZ. Rodgers and Bhattacharyya [2001] found that triplicated phase waveforms that sample beneath the western MOMA stations require a LVZ. In addition, Schultz et al. [1993] observed a peak conductivity at \sim 280 km beneath the central Canadian Shield, which is consistent with a seismic low-velocity zone.

[26] We modeled the 270–320 km phases (Figure 6) with a variety of velocity structures and found that a velocity discontinuity of \sim 5.5% is required beneath the eastern stations. The amplitude of the 320-km phase beneath the western stations is not particularly robust, but it implies a weaker discontinuity or

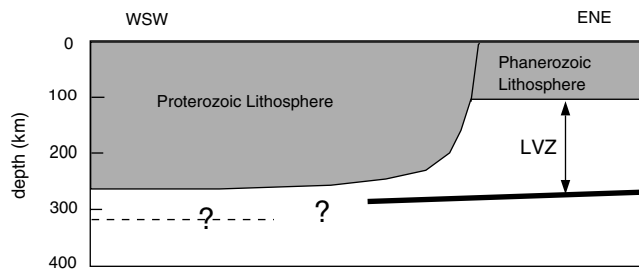


Figure 7. A schematic cross section along the MOMA array showing variations of lithospheric structure and a LVZ across the eastern boundary of the North American keel. The lithosphere is shaded with a thin solid line separating the Proterozoic lithosphere which is thick but confined above 300 km from the Phanerozoic lithosphere which is ~ 100 km thick [Grand *et al.*, 1997; van der Lee and Nolet, 1997]. The bottom of the lithosphere is the top of a LVZ according to Hirth *et al.* [2000], who proposed that it is the transition from dry to wet mantle. The base of the LVZ is plotted according to our observations of P to S conversions, which occurs at ~ 320 km beneath western bins (dashed line) and 270–280 km beneath eastern bins (thick black line).

gradient than is observed in the east. We also examined both radial and transverse receiver functions for back azimuthal variations that might diagnose the presence of anisotropy at this discontinuity or at shallower depths. Unfortunately, however, the back azimuthal distribution of the data was too limited to yield meaningful constraints.

[27] If the phases are generated at the base of a LVZ, our observations suggest a stronger and shallower LVZ outside the keel and a weaker and deeper LVZ beneath the keel (Figure 7). Water enrichment is one mechanism that could produce such a LVZ. Based on mantle conductivity profiles, Hirth *et al.* [2000] proposed a transition from hydrated mantle to dehydrated mantle at the base of the lithosphere beneath both oceanic and continental regions, with this transition occurring at depths of ~ 250 km beneath cratons and ~ 100 km beneath oceans. This boundary would represent the top of a sublithospheric LVZ, with greater water content providing the mechanism for lower strength and wave speeds. The origin of a sharp lower boundary to such a LVZ is less clear. Release of volatiles from a dehydrating phase transformation is one possibility, particularly if the depth of the dehydration boundary could be increased beneath the western stations due to a cooler subcratonic mantle geotherm, although the lack of significant topography on the 410-km discontinuity indicates that strong temperature variations across the region do not persist into the transition zone. However, while a number of phases may store water in the deep upper mantle [e.g., Thompson, 1992], no obvious candidate for a dehydration boundary at the correct temperature and pressure conditions appears to exist. The phase transitions from the orthorhombic to high- P monoclinic phase in Mg-Fe pyroxene [Woodland, 1998] or from coesite to stishovite [Williams and Revenaugh, 2000] have also been offered as explanations for discontinuities in this depth range. However, assuming that temperatures decrease toward the thick cratonic keel, these transitions would shallow from east to west [Woodland, 1998; Liu *et al.*, 1996], opposite to the observed increase in discontinuity depth. Alternatively, the discontinuity could represent the transition from dislocation creep, which would produce anisotropic mantle fabrics at shallower depth, to diffusion creep, which would result in a lack of elastic anisotropy at greater depths. The likely temperature and pressure dependence of the diffusion creep/dislocation creep boundary [Karato and Wu, 1992; Karato, 1992] would result in a deeper discontinuity with cooler temperatures below the subcratonic lithosphere. A zone of

enhanced mechanical weakness and localized strain associated with this boundary would be likely [Karato and Wu, 1992].

6. Conclusions

[28] Crustal velocity structures with one or two sedimentary layers and one crustal basement layer were obtained by matching synthetic P_s conversions and reverberations from the Moho to observed crustal receiver function stacks. The thickest crust Moho lies beneath the western Appalachians and extends just to the west of the Appalachian Front. Crustal thickness is roughly correlated with topography over ~ 300 km length scales, and given the magnitude of the observed crustal root (4–6 km), the density contrast between the crustal root and mantle must be small (< 200 kg/m 3) in order to balance the topography in local isostatic equilibrium.

[29] Receiver function stacks beneath the MOMA array are characterized by a flat discontinuity at 410 km, which indicates that cold temperatures related to the North America continental keel are largely confined in the upper mantle and argues for a neutrally buoyant keel. In the upper mantle, phases from a continuous discontinuity at depths of 270–280 km were observed beneath the eastern stations (bins 10–19), with the depth of the phase increasing toward the west. Beneath the western stations (bins 1–7), scattering is more complex, but a laterally continuous discontinuity appears to occur at depths of ~ 320 km. We propose that the lateral transition between the stronger, shallower discontinuity in bins 10–19 and the weaker, deeper discontinuity in bins 1–7 represents a variation in mantle structure associated with the eastern edge of the keel. These phases may be produced by an increase in velocity at the base of a mechanically weak LVZ. The variation of depth and strength of the upper mantle discontinuity beneath the MOMA array suggests a stronger, shallower, and thicker asthenosphere outside the craton and a weaker, deeper, and thinner asthenosphere beneath the craton.

[30] **Acknowledgments.** We would like to thank Steve Grand for his mantle velocity model and his constructive review. Thanks also to an anonymous reviewer and to Anne Sheehan, Tom Owens, Yang Shen, and Don Forsyth for their helpful perspectives. We are very grateful to everyone who worked on the MOMA experiment, including the staff of the PASSCAL Instrument Center at Lamont-Doherty Earth Observatory and Matt Fouch, Tim Clarke, Ghassan Al-Eqabi, Keith Koper, Erich Roth, Lynn Salvati, Patrick Shore, Raul Valenzuela, and Julie Zaslow. Many thanks to the individuals and institutions who allowed us to build stations on their property, in particular, James Amory, James Wheeler, and Justin West. Funding for the MOMA experiment was provided by the National Science Foundation under awards EAR93-19324, EAR93-15971, and EAR93-15825; additional funding for this study was provided by award EAR96-14705.

References

- Agnon, A., and M. S. T. Bukowski, δs at high pressure and $d \ln V_s / d \ln V_p$ in the lower mantle, *Geophys. Res. Lett.*, **17**, 1149–1152, 1990.
- Akaogi, M., E. Ito, and A. Navrotsky, Olivine-modified spinel-spinel transitions in the system Mg $_2$ SiO $_4$ –Fe $_2$ SiO $_4$: Calorimetric measurements, thermochemical calculation, and geophysical application, *J. Geophys. Res.*, **94**, 15,671–15,685, 1989.
- Ammon, C. J., The isolation of receiver effects from teleseismic P waveforms, *Bull. Seismol. Soc. Am.*, **81**, 2504–2510, 1991.
- Anderson, D. L., The deep structure of continents, *J. Geophys. Res.*, **84**, 7555–7560, 1979.
- Bina, C. R., and B. J. Wood, Olivine-spinel transitions: Experimental and thermodynamic constraints and implications for the nature of the 400-km discontinuity, *J. Geophys. Res.*, **92**, 4853–4866, 1987.
- Bostock, M. G., Anisotropic upper-mantle stratigraphy and architecture of slave craton, *Nature*, **390**, 392–395, 1997.
- Boyd, F. R., Compositional distinction between oceanic and cratonic lithosphere, *Earth. Planet. Sci. Lett.*, **96**, 15–26, 1989.
- Braille, L. W., Crustal structure of the continental interior, in *Geophysical Framework of the Continental United States*, edited by L. C. Pakiser and W. D. Mooney, *Mem. Geol. Soc. Am.*, **172**, 285–315, 1989.

- Braile, L. W., W. J. Hinze, R. R. B. von Frese, G. Randy Keller, Seismic properties of the crust and uppermost mantle of the conterminous United States and adjacent Canada, in *Geophysical Framework of the Continental United States*, edited by L. C. Pakiser and W. D. Mooney, *Mem. Geol. Soc. Am.*, 172, 655–680, 1989.
- Costain, J. K., R. D. Hatcher Jr., C. Coruh, L. P. Thomas, S. R. Taylor, J. J. Litehiser, and I. Zietz, Geophysical characteristics of the Appalachian crust, in *The Geology of North America*, vol. F-2, *The Appalachian-Ouachita Orogen in the United States*, edited by R. D. Hatcher Jr., W. A. Thomas, and G. W. Viele, pp. 385–416, Geol. Soc. of Am., Boulder, Colo., 1989.
- Dueker, K. G., and A. F. Sheehan, Mantle discontinuity structure from midpoint stacks of converted *P* to *S* waves across the Yellowstone hotspot track, *J. Geophys. Res.*, 102, 8313–8327, 1997.
- Dueker, K. G., and A. F. Sheehan, Mantle discontinuity structure beneath the Colorado Rocky Mountains and High Plains, *J. Geophys. Res.*, 103, 7153–7169, 1998.
- Dziewonski, A. M., and D. L. Anderson, Preliminary reference Earth model (PREM), *Phys. Earth Planet. Inter.*, 25, 297–356, 1981.
- Fischer, K. M., M. E. Wyssession, T. J. Clarke, M. J. Fouch, G. I. Al-eqabi, P. J. Shore, R. W. Valenzuela, A. Li, and J. M. Zaslów, The 1995–1996 Missouri to Massachusetts broadband seismometer deployment, *IRIS Newsl.*, 15, 6–9, 1996.
- Flawn, P. T., D. M. Kinney, and Basement Rock Project Committee, Basement map of North America between latitudes 24° and 60° N, U.S. Geol. Surv., Washington, D. C., 1967.
- Gaherty, J. B., and T. H. Jordan, Lehmann discontinuity as the base of an anisotropic layer beneath continents, *Science*, 268, 1468–1471, 1995.
- Gaherty, J. B., M. Kato, and T. H. Jordan, Seismological structure of the upper mantle: A regional comparison of seismic layering, *Phys. Earth Planet. Inter.*, 110, 21–41, 1999.
- Grand, S. P., Mantle shear structure beneath the Americas and surrounding oceans, *J. Geophys. Res.*, 99, 11,591–11,621, 1994.
- Grand, S. P., R. D. van der Hilst, and S. Widiyantoro, Global seismic tomography: A snapshot of convection in the Earth, *GSA Today*, 7, 1–7, 1997.
- Hales, A. L., Upper mantle models and the thickness of the continental lithosphere, *Geophys. J. Int.*, 105, 355–363, 1991.
- Hatcher, R. D., Jr., Tectonic synthesis of the U.S. Appalachians, in *The Geology of North America*, vol. F-2, *The Appalachian-Ouachita Orogen in the United States*, edited by R. D. Hatcher, Jr., W. A. Thomas, and G. W. Viele, pp. 511–535, Geol. Soc. of Am., Boulder, Colo., 1989.
- Hawman, R. B., and R. A. Phinney, Structure of the crust and upper mantle beneath the great valley and Allegheny Plateau of eastern Pennsylvania, 1, Comparison of linear inversion methods for sparse wide-angle reflection data, *J. Geophys. Res.*, 97, 371–391, 1992.
- Hinze, W. J., The crust of the northern U.S. craton: A search for beginnings, in *Basement and Basins of Eastern North America*, edited by B. A. van der Pluijm and P. A. Catacosinos, *Spec. Pap. Geol. Soc. Am.*, 308, 181–201, 1996.
- Hirth, G., R. Evans, and D. Chave, Comparison of continental and oceanic mantle electrical conductivity: Evidence for a dry Archean lithosphere, *Geochem. Geophys. Geosyst.*, 1(Article), 2000GC000048 [4373 words], 2000.
- Hittelman, A. M., J. O. Kinsfather, and H. Meyers, *Geophysics of North America* [CD-ROM], Natl. Geophys. Data Cent., Boulder, Colo., 1990.
- Hoffman, P. F., Precambrian geology and tectonic history of North America, in *The Geology of North America*, vol. A, *Overview*, edited by A. W. Bally and A. R. Palmer, pp. 447–512, Geol. Soc. of Am., Boulder, Colo., 1989.
- Hutchinson, D. R., J. A. Grow, and K. D. Klitgord, Crustal structure beneath the southern Appalachians: Nonuniqueness of gravity modeling, *Geology*, 11, 611–615, 1983.
- Isaak, D. G., High-temperature elasticity of iron-bearing olivines, *J. Geophys. Res.*, 97, 1871–1885, 1992.
- James, D. E., T. J. Smith, and J. S. Steinhart, Crustal structure of the Middle Atlantic States, *J. Geophys. Res.*, 73, 1983–2007, 1968.
- Jordan, T. H., Composition and development of the continental tectosphere, *Nature*, 274, 544–548, 1978.
- Jordan, T. H., Structure and formation of the continental tectosphere, *J. Petrol.*, *Special Lithosphere Issue*, 11–37, 1988.
- Karato, S., On the Lehman discontinuity, *Geophys. Res. Lett.*, 19, 2255–2258, 1992.
- Karato, S., and P. Wu, Rheology of the upper mantle: A synthesis, *Science*, 260, 771–778, 1992.
- Karner, G. D., and A. B. Watts, Gravity anomalies and flexure of the lithosphere at mountain ranges, *J. Geophys. Res.*, 88, 10,449–10,477, 1983.
- Katsura, T., and E. Ito, The system Mg₂SiO₄–Fe₂SiO₄ at high pressure and temperatures: Precise determination of stabilities of olivine, modified spinel, and spinel, *J. Geophys. Res.*, 94, 15,663–15,670, 1989.
- Keller, G. R., C. M. Snelson, A. F. Sheehan, and K. G. Dueker, Geophysical studies of crustal structure in the Rocky Mountain region: A review, *Rocky Mt. Geol.*, 33, 217–228, 1998.
- Kennett, B. L. N., E. R. Engdahl, and R. Buland, Constraints on seismic velocities in the Earth from travel times, *Geophys. J. Int.*, 122, 108–124, 1995.
- Klitgord, K. D., D. R. Hutchinson, and H. Schouten, U.S. Atlantic continental margin; Structural and tectonic framework, in *The Atlantic Continental Margin, U.S.*, edited by R. E. Sheridan and J. A. Grow, pp. 19–51, Geol. Soc. of Am., Boulder, Colo., 1989.
- Langston, C. A., Structure under Mount Rainier, Washington, inferred from teleseismic body waves, *J. Geophys. Res.*, 84, 4749–4762, 1979.
- Langston, C. A., An integrated study of crustal structure and regional wave propagation for southeastern Missouri, *Bull. Seismol. Soc. Am.*, 84, 105–118, 1994.
- Lehmann, I., *S* and the structure of the upper mantle, *Geophys. J. R. Astron. Soc.*, 4, 124–138, 1961.
- Leven, J. H., I. Jackson, and A. E. Ringwood, Upper mantle seismic anisotropy and lithospheric decoupling, *Nature*, 289, 234–239, 1981.
- Li, A., K. M. Fischer, M. E. Wyssession, and T. J. Clarke, Mantle discontinuities and temperature under the North American continental keel, *Nature*, 395, 160–163, 1998.
- Liu, J., L. Topor, J. Zhang, A. Navrotsky, and R. C. Liebermann, Calorimetric study of the coesite-stishovite transformation and calculation of the phase boundary, *Phys. Chem. Miner.*, 23, 11–16, 1996.
- Marshak, S., and B. A. van der Pluijm, The U. S. continental interior, in *Earth Structure: An Introduction to Structural Geology and Tectonics*, edited by B. A. van der Pluijm and S. Marshak, pp. 465–472, McGraw-Hill, New York, 1997.
- McNutt, M., Implications of regional gravity for state of stress in the Earth's crust and upper mantle, *J. Geophys. Res.*, 85, 6377–6396, 1980.
- Mooney, W. D., and L. W. Braile, The seismic structure of the continental crust and upper mantle of North America, in *The Geology of North America*, vol. A, *Overview*, edited by A. W. Bally and A. R. Palmer, pp. 39–52, Geol. Soc. of Am., Boulder, Colo., 1989.
- Mooney, W. D., G. Laske, and T. G. Masters, Crust 5.1: A global crustal model at 5° × 5°, *J. Geophys. Res.*, 103, 727–747, 1998.
- Musacchio, G., W. D. Mooney, J. H. Luetgert, and N. I. Christensen, Composition of the crust in the Grenville and Appalachian provinces of North America inferred from *V_p/V_s* ratios, *J. Geophys. Res.*, 102, 15,225–15,241, 1997.
- Owens, T. J., and S. C. Crosson, Shallow structure effects on broadband teleseismic *P* waveforms, *Bull. Seismol. Soc. Am.*, 78, 96–108, 1988.
- Owens, T. J., A. A. Nyblade, H. Gurrrola, and C. A. Langston, Mantle transition zone structure beneath Tanzania, East Africa, *Geophys. Res. Lett.*, 27, 827–830, 2000.
- Pratt, T., R. Culotta, E. Hauser, D. Nelson, L. Brown, S. Kaufman, and J. Oliver, Major Proterozoic basement features of the eastern midcontinent of North America revealed by recent COCORP profiling, *Geology*, 17, 505–509, 1989.
- Rankin, D. W., Continental margin of the eastern United States: Past and present, in *Phanerozoic Evolution of North America Continent-Ocean Transitions*, edited by R. C. Speed, pp. 129–218, Geol. Soc. of Am., Boulder, Colo., 1994.
- Rankin, D. W., et al., Proterozoic rocks east and southeast of the Grenville front, in *The Geology of North America*, vol. C-2, *Precambrian: Conterminous U.S.*, edited by J. C. Reed et al., pp. 335–461, Geol. Soc. of Am., Boulder, Colo., 1993.
- Rast, N., The evolution of the Appalachian chain, in *The Geology of North America—An Overview*, edited by A. W. Bally and A. R. Palmer, pp. 323–348, Geol. Soc. of Am., Boulder, Colo., 1989.
- Revenaugh, J., and T. H. Jordan, Mantle layering from *ScS* reverberations, 3, The upper mantle, *J. Geophys. Res.*, 96, 19,781–19,810, 1991.
- Revenaugh, J., and S. A. Sipkin, Mantle discontinuity structure beneath China, *J. Geophys. Res.*, 99, 21,911–21,927, 1994.
- Rodgers, A., and J. Bhattacharyya, Upper mantle shear and compressional velocity structure of the central US craton: Shear wave low-velocity zone and anisotropy, *Geophys. Res. Lett.*, 28, 383–386, 2001.
- Schmidberger, S. S., and D. Francis, Nature of the mantle roots beneath the North American craton: Mantle xenolith evidence from Somerset Island kimberlites, *Lithos*, 48, 195–216, 1999.
- Schultz, A., R. D. Kurtz, A. D. Chave, and A. G. Jones, Conductivity discontinuities in the upper mantle beneath a stable craton, *Geophys. Res. Lett.*, 20, 2941–2944, 1993.
- Shearer, P. M., Constraints on upper mantle discontinuities from observations of long-period reflected and converted phases, *J. Geophys. Res.*, 96, 18,147–18,182, 1991.
- Shearer, P. M., M. P. Flanagan, and M. A. H. Hedlin, Experiments in migration processing of *SS* precursor data to image upper mantle discontinuity structure, *J. Geophys. Res.*, 104, 7229–7242, 1999.

- Sheehan, A. F., G. A. Abers, C. H. Jones, and A. L. Lerner-Lam, Crustal thickness variations across the Colorado Rocky Mountains from teleseismic receiver functions, *J. Geophys. Res.*, *100*, 20,391–20,404, 1995.
- Sheehan, A. F., P. M. Shear, H. J. Gilbert, and K. G. Dueker, Seismic migration processing of P - SV converted phases for mantle discontinuity structure beneath the Snake River Plain, western United States, *J. Geophys. Res.*, *105*, 19,055–19,065, 2000.
- Shen, Y., S. C. Solomon, I. T. Bjarnason, and C. J. Wolfe, Seismic evidence for a lower mantle origin of the Iceland plume, *Nature*, *395*, 62–65, 1998.
- Shumaker, R. C., and T. H. Wilson, Basement structure of the Appalachian foreland in west Virginia: Its style and effect on sedimentation, in *Basement and Basins of Eastern North America*, edited by B. A. van der Pluijm and P. A. Catocinos, *Spec. Pap. Geol. Soc. Am.*, *308*, 139–168, 1996.
- Sleep, N. H., Monterey hotspot track: A long-lived mantle plume, *J. Geophys. Res.*, *95*, 21,983–21,990, 1990.
- Thompson, A. B., Water in the Earth's upper mantle, *Nature*, *358*, 295–302, 1992.
- Van der Hilst, R. D., S. Widiyantoro, and E. R. Engdahl, Evidence for deep mantle circulation from global tomography, *Nature*, *386*, 578–584, 1997.
- van der Lee, S., and G. Nolet, Upper mantle S velocity structure of North America, *J. Geophys. Res.*, *102*, 22,815–22,838, 1997.
- Williams, Q., and J. Revenaugh, The X-discontinuity: A signature of deep fluid flow and free silica in the sub-continental mantle, *Eos Trans. AGU*, *81*(48), Fall Meet. Suppl., F922, 2000.
- Woodland, A. B., The orthorhombic to high- P monoclinic phase transition in Mg-Fe pyroxenes: Can it produce a seismic discontinuity?, *Geophys. Res. Lett.*, *25*, 1241–1244, 1998.
- Yuan, X., J. Ni, R. Kind, J. Mechie, and E. Sandvol, Lithospheric and upper mantle structure of southern Tibet from a seismological passive source experiment, *J. Geophys. Res.*, *102*, 27,491–27,500, 1997.
-
- K. M. Fischer, Department of Geological Sciences, Brown University, P.O. Box 1846, Providence, Rhode Island RI 02912, USA. (karen_fischer@brown.edu)
- A. Li, Department of Geology and Geophysics, Woods Hole Oceanographic Institution, Woods Hole, MA 02543, USA. (aibing@whoi.edu)
- S. van der Lee, Institute of Geophysics, ETH Honggerberg (HPP), CH-8093, Zurich, Switzerland. (suzan@tomo.ig.erdw.ethz.ch)
- M. E. Wysession, Department of Earth and Planetary Sciences, Washington University, One Brookings Dr., St. Louis, MO 63130-4899, USA. (michael@wucore.wustl.edu)

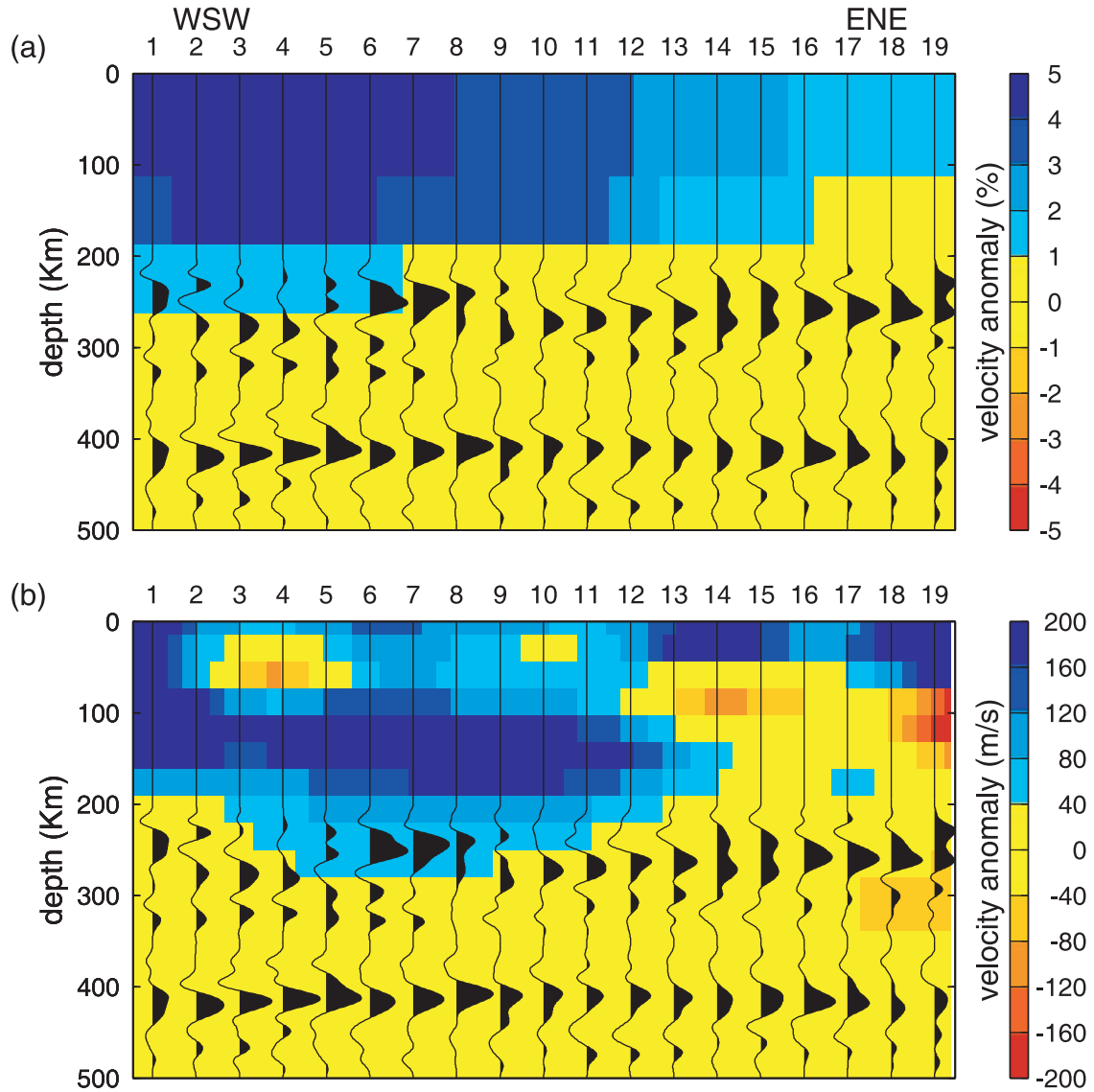


Figure 6. Receiver functions including conversion depths at 300 and 410 km on a background of velocity anomaly from (a) the Grand model and (b) the NA98 model. Data in the 200–350 km depth range are stacked with move out corrections for conversions at 300 km, and data in the 350–500 km depth range are stacked with move out corrections for conversions at 410 km. Earlier arriving phases are not shown. The keel is imaged by a broad lateral gradient in the Grand model, while it is a sharper feature in the NA98 model. The keel is confined above 300 km in both models, which is consistent with the relatively flat discontinuity at 410 km. Receiver function stacks are filtered with a 0.05–1 Hz band pass.